Biophysical Reports

ARTICLE

A transistor model for the cystic fibrosis transmembrane conductance regulator

William D. Hunt,[1,*] Nael A. McCarty,[2] Eduardo Martinez Marin,[1] Ryan S. Westafer,[3] Phillip R. Yamin,[1] Guiying Cui,[2] Andrew W. Eckford,[4] and Douglas R. Denison[3]

[1]Georgia Institute of Technology, Atlanta, Georgia; [2]Emory University School of Medicine, Atlanta, Georgia; [3]GTRI, Atlanta, Georgia; and [4]York University, Toronto, Ontario, Canada

ABSTRACT In this paper we present a transistor circuit model for cystic fibrosis transmembrane conductance regulator (CFTR) that seeks to map the functional form of CFTR both in wild type and mutants. The circuit architecture is configured so that the function, and as much as possible the form, faithfully represents what is known about CFTR from cryo-electron microscopy and molecular dynamics. The model is a mixed analog-digital topology with an AND gate receiving the input from two separate ATP-nucleotide-binding domain binding events. The analog portion of the circuit takes the output from the AND gate as its input. The input to the circuit model and its noise characteristics are extracted from single-channel patch-clamp experiments. The chloride current predicted by the model is then compared with single-channel patch-clamp recordings for wild-type CFTR. We also consider the patch-clamp recordings from CFTR with a G551D point mutation, a clinically relevant mutant that is responsive to therapeutic management. Our circuit model approach enables bioengineering approaches to CFTR and allows biophysicists to use efficient circuit simulation tools to analyze its behavior.

WHY IT MATTERS The dysfunction of cystic fibrosis transmembrane conductance regulator (CFTR), induced by mutations, is responsible for the disease cystic fibrosis. While much is known about the functional aspects of CFTR, significant gaps remain in our knowledge and understanding. Paths toward a fuller understanding of this membrane channel include structural studies, molecular dynamics simulations, and single-channel patch-clamp studies of function that may be enhanced using modeling approaches as described here. The circuit is, in the parlance of electronics, a voltage-to-current converter. For a biophysical approach, one could think of the circuit as an energy-to-current converter. The computational efficiency and complexity of circuit simulation tools, such as LTspice and Cadence, facilitate the investigation of wild-type CFTR and its mutations.

INTRODUCTION

Ever since the cloning of the cystic fibrosis transmembrane conductance regulator (CFTR) gene in 1989 (1), the corresponding protein, CFTR, has been studied extensively because it is the locus of the primary defect in the disease cystic fibrosis (CF). CF is a multiple-organ disease, affecting primarily the respiratory and digestive tracts, with substantial impact on the quality and length of life of individuals affected by the disease. The genetic complexity of CF is substantial, with nearly 2000 CFTR mutations identified (2) and more than 300 identified as disease-causing (3). While recent years have seen the development of novel therapeutics for a subset of these mutations leading to enhanced surface expression and activity of CFTR in epithelial cells, not all genotypes are responsive. Hence, further understanding the functional mechanisms by which CFTR activity leads to chloride secretion remains critical for developing further therapeutic approaches. Understanding CFTR is challenging in part because it is unique. While it is built upon the structural plan of the ATP-binding cassette (ABC) transporter superfamily, it mainly functions as a channel rather than a transporter (4). The ABC transporter superfamily represents an ancient lineage of transmembrane proteins found in all organisms. These typically have four domains: two nucleotide-binding domains (NBDs) and two transmembrane domains (TMDs) (5). CFTR bears an additional domain, the regulatory R domain, which must

Submitted December 8, 2022, and accepted for publication April 7, 2023.

*Correspondence: bill.hunt@ece.gatech.edu

Editor: Jorg Enderlein.

https://doi.org/10.1016/j.bpr.2023.100108

be phosphorylated in order for the channel to function. Other ABC transporter proteins move a preferred substrate in a single direction across the membrane with typically a strict stoichiometric relationship between the amount of substrate transported and the number of ATP molecules consumed. The binding of ATP at, typically, two distinct sites, across the interface of the two NBDs as they dimerize, induces conformational change in the TMDs. The hydrolysis of ATP leads to the translocation of the substrate across the membrane; hence, traditional ABC transporters are primary active transporters (6). CFTR, on the other hand, evolved to use ATP to form a pathway for chloride or bicarbonate ions to cross the plasma membrane whereby ions flow passively down their electrochemical gradient until ATP is hydrolyzed and the channel closes (7). CFTR uses a modified "alternating access" transport mechanism (8) whereby the rapid conformational changes more closely associated with canonical ABC transporters that regulate accessibility to the substrate-binding pocket from only one side of the membrane at a time are altered in order to form a continuous pathway across the membrane—on the time scale of a second (9). In the traditional alternating access model, the substrate has access to the binding site from inside the cell (inward-facing state) or from outside the cell (outward-facing state) but not both at the same time (10). In CFTR, the inner gate that would typically block diffusion from the substrate-binding pathway into the cell in the equivalent of the outward-facing state is degraded such that the substrate transport pathway is no longer closed to the inside, thereby enabling diffusion of substrate (chloride) across the membrane. CFTR also bears a series of intraprotein residue-residue interactions that stabilize the open state, further slowing the pump-like action of canonical ABC transporters (7). The cycle of conformational changes in ABC transporters, such as CFTR, are driven by the binding and hydrolysis of ATP at the cytosolic NBDs. One of CFTR's NBDs bears a degenerate ATP-binding site, a feature found in some transporters from the ABCC class (11), and thus CFTR can only hydrolyze ATP at one of the two binding sites.

CFTR also possesses a unique regulatory domain (R domain) represented by approximately 240 residues found between NBD_1 and TMD_2 (1). The R domain is an intrinsically disordered domain and appears to have evolved from the incorporation of intronic sequence following the loss of an RNA splicing site (12). While the mechanism by which the R domain regulates CFTR function remains unclear, it tightly regulates channel function based on the phosphorylation state of multiple residues in this domain (13,14).

While CFTR is clearly a member of the ABC transporter superfamily, its unique function as an ion channel has enabled this complex protein to be studied at very high resolution, in both amplitude and time using a variety of electrophysiological techniques. In combination with cell biological techniques, electrophysiological approaches have been used to characterize and classify many clinically relevant mutations as they have been identified (15–17). In combination with site-directed mutagenesis, electrophysiological experiments led to the identification of many residues critical to CFTR function (18). Structural data from cryo-electron microscopy combined with molecular dynamics techniques are helping the community to gain a better understanding of the locations of these key functional residues within CFTR. It is hoped that this work may assist in the development of new therapeutics. In short, there is still much work to be done in this area.

In this paper we present a transistor circuit model of the CFTR membrane channel. The importance of circuit models to represent electrophysiological events has been clear at least since Hodgkin and Huxley (19). They were awarded the 1963 Nobel Prize in Physiology and Medicine for the development, after more than a decade of research, of a circuit model which provides insight into the underlying biophysical properties that are central to the operation of axons. A key aspect of the Hodgkin-Huxley (H-H) model is the set of nonlinear differential equations used to express transport of K^+ and Na^+ through ion-specific voltage-gated channels. Over the years since there has been much work on electronic modeling of neuronal processes (20–32). but the H-H model remains the workhorse of neurophysiology (33). The H-H model is a macroscopic one and was developed from clever experimental measurements and patch techniques (34). It is interesting to note, and germane to the present paper, that although Hodgkin and Huxley reported their seminal work in 1952 (19,35–38), it was not until 1981 that the controversy regarding the role of these individual membrane channels in cellular electrical activity was settled by the paper from Hamill et al. providing single-channel patch-clamp measurements (39). Roughly 30 years passed between Hodgkin and Huxley's macroscopic model of axon electrical activity and an understanding of the underlying microscopic foundation.

Let us examine the usefulness and proper fit of transistors to the modeling of membrane channel function and in particular CFTR. Ions such as K^+,Na^+,Ca^{2+}, and Cl^- move back and forth across the plasma membrane of the eukaryotic cell by the forces of diffusion and drift. These forces are the same physical forces which drive electrons and holes in semiconductor devices such as the bipolar junction transistor (BJT). To the untrained eye, it may appear that utilizing transistors as

components in the CFTR model glosses over much of the beautiful physics associated with these structures. However, circuit modeling programs such as Cadence (www.cadence.com) and LTspice (Analog Devices) can incorporate a multitude of physics modeling for each individual component. For example, Verilog-A is a programming language used for the modeling of transistors for analog integrated circuits, and some of these models have up to 2000 lines of code. These model equations include both linear and nonlinear aspects of the transistor behavior. Given the complexity of the physics available within a transistor model, our approach should be seen as a technique complementary to molecular dynamics. Although it might seem better in electronics to keep track of every electron, every hole, and impurities and defects within a semiconductor crystal, what has been found since the beginning (40) is that models which capture the essential device physics and are accurate in their predictions of transistor behavior are of tremendous value. These modeling tools are quite accurate. One could not fabricate the chips of today, which contain billions of transistors, without simulation tools that predict the device behavior while also including manufacturing variations.

Furthermore, although many applications of BJTs are in the device's linear region of operation, there are many for which the nonlinear properties of the transistor must be considered. As such, BJTs are excellent components to be included in models for cellular electrophysiological function and, more importantly here, individual membrane channel function. There have been a number of researchers who have investigated the use of transistors for single-channel modeling (41–48). To the best of our knowledge this is the first report of a transistor model for CFTR, a unique channel regulated by the combination of post-translational modification (via phosphorylation), ligand binding (ATP), and hydrolysis of that ligand, thus resulting in a cyclical gating scheme.

Concisely, the main contribution of this paper is a transistor model for the membrane channel CFTR. The circuit-component-level representation facilitates the modification of transistor parameters so as to mimic the impact of various mutations of CFTR. The output of our circuit model will be compared with single-channel patch-clamp experiments.

MATERIALS AND METHODS

Preparation of oocytes and cRNA

For electrophysiology experiments, Human CFTR cRNAs used in this study were prepared from constructs encoding the wild-type (WT) CFTR gene in the pGEMHE vector. The G551D mutant was generated using the Quikchange site-directed mutagenesis kit (Stratagene, La Jolla, CA) and the entire open reading sequenced as previously reported (49). *Xenopus laevis* oocytes were injected with 0.5–10 ng of CFTR cRNAs based on the standard experimental protocol, and were incubated at 17°C in modified Liebovitz's L-15 medium with addition of HEPES (pH 7.5), penicillin, and streptomycin. Electrophysiology experiments were performed 24–96 h following injection of cRNAs. Protocols for frog handling and oocyte collection were based on and adhere to NIH guidelines, and have been approved by the Institutional Animal Care and Use Committee of Emory University (49).

Electrophysiology

All electrophysiology pipettes used for inside-out single-channel recordings were pulled from borosilicate glass (Sutter Instrument, Novato, CA) and pipette resistances were roughly 10 MΩ after filling with chloride-containing pipette solution: 150 mM *N*-methyl-D-glucamine chloride (NMDG-Cl), 5 mM $MgCl_2$, 10 mM TES (pH 7.5), as previously reported (50,51). Oocytes were shrunk in hypertonic solution followed by manual removal of the vitelline membrane before electrophysiology experiments. Inside-out patches were excised from CFTR-expressing oocytes, and CFTR channels were activated in cytoplasmic solution containing 150 mM NMDG-Cl, 1.1 mM $MgCl_2$, 2 mM Tris-EGTA, 10 mM TES, 1 mM adenosine 5′-triphosphate magnesium (MgATP), and 127 U/mL protein kinase A (PKA) (pH 7.45). All electrophysiology experiments were carried out at room temperature (22°C–23°C) using an Axopatch 200B amplifier. Data were recorded to digital tape, then played back and acquired to a computer using Clampfit 9.0 (www.moleculardevices.com). Single-channel data were analyzed with Clampfit 10.2 software (49,52). The structure and state model for CFTR are shown in Fig. 1.

Source of reagents

Unless otherwise noted, all reagents were obtained from MilliporeSigma (St. Louis, MO). L-15 medium was obtained from Gibco/BRL (Gaithersburg, MD). CFTRinh172 was purchased from Calbiochem (Burlington, MA) and made as 50 mM stock in DMSO for future use. PKA was used at, or diluted from, 127.6 U/mL to indicated final concentrations for patch-clamp experiments (Promega, Madison, WI). VX-770 was initially made as a 10 mM stock solution dissolved in DMSO (Selleckchem, Houston, TX). All chemicals used in this study were diluted to their final concentration in the relevant recording solution immediately prior to use (51).

CFTR transistor circuit model

CFTR membrane channels receive input energy from two ATP molecules binding directly at the interface of the NBD_1 and NBD_2 dimer and use this energy to open the CFTR pore so that chloride ions may flow through the channel. One of the ATP molecules, which we will call ATP_1, binds ATP-binding site #1 (ABS1, comprising sequences from both NBD_1 and NBD_2) and stays bound for a considerable period of time, since ATP hydrolysis at ABS1 is defective because of mutations common across the ABC lineage that includes CFTR. The other ATP molecule, which we will call ATP_2, binds ABS2 (also comprising sequences from both NBD_1 and NBD_2), and this keeps the WT-CFTR channel open for roughly 600 ms on average. Once ATP_2 is hydrolyzed, the channel rapidly closes. It is theorized that the combination of the two ATP molecules binding to ABS1 and ABS2 in WT CFTR results in a torquing of the protein around a fulcrum point roughly in the midpoint of the membrane (7). This torque causes a rotation of the membrane domains of the protein

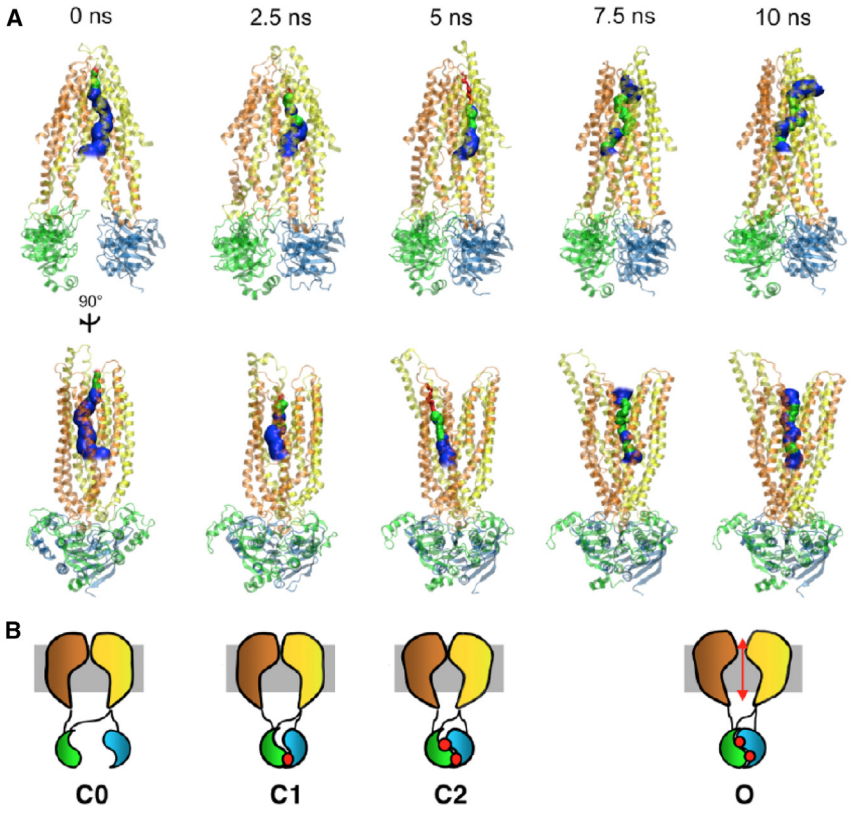

FIGURE 1 The structure and state space representation for CFTR. (*A*) The protein structure from closed state (C0) to open state (O). (*B*) State model representations. Brown and yellow are representations of two halves of the transmembrane portion of the protein. Green and blue configured in the Yin-Yang symbol represent NBD_1 and NBD_2. The red circles represent the bound ATP molecules. Chloride current is shown by the red arrow (53).

about a center of mass with a radius of gyration, R_G (54). This results in an opening of a pore in the CFTR membrane channel. The subsequent effect of this is to allow for the transport of Cl^- ions.

One of our metrics of circuit model efficacy is to have the predictions provided by the circuit to faithfully represent single-channel WT and the G551D mutant patch-clamp single-channel recordings. For the single-channel recordings presented here, the chloride concentration outside and inside the cell are the same. As such, the Nernst potential for Cl^- is zero. Slight modifications would need to be made to the model to allow for a non-zero Nernst potential and for the possibility of other ions being transported through CFTR such as bicarbonate (HCO_3). In this paper we will restrict our discussions to the circuit of Fig. 2, which is a model of CFTR under the experimental conditions of our single-channel patch-clamp measurements.

The analog portion of the circuit, shown in Fig. 2, is a voltage-to-current converter representing the mechanism within the CFTR membrane channel in which the energy associated with ATP binding results in Cl^- current flow. What is driving the CFTR channel is the two ATP molecules being bound at the same time to the NBD regions. As such, input to the analog portion of the circuit is very much like an AND gate in a digital circuit. Both inputs have to be high to produce a positive output. The input section of the model is shown on the left side of Fig. 2 as a digital circuit. The voltage

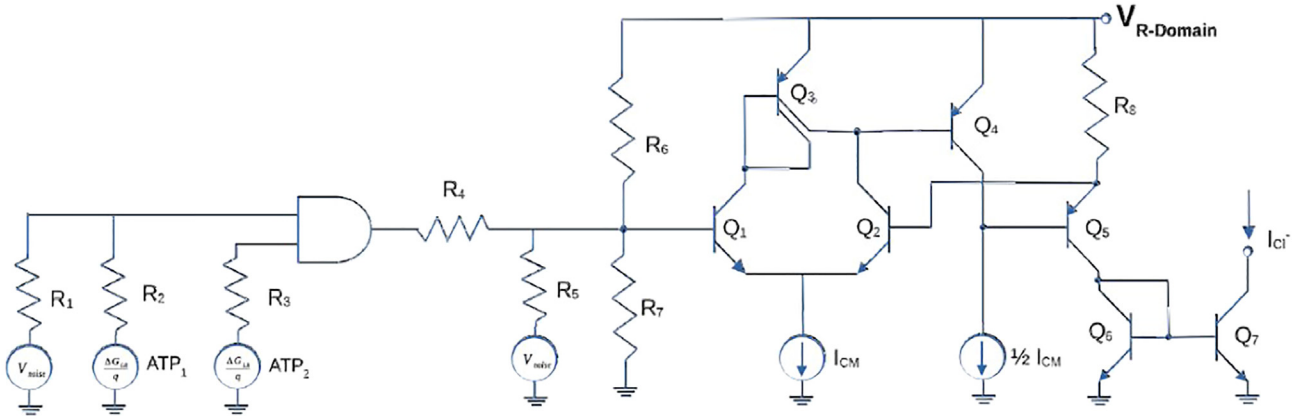

FIGURE 2 The mixed analog-digital circuit model for CFTR.

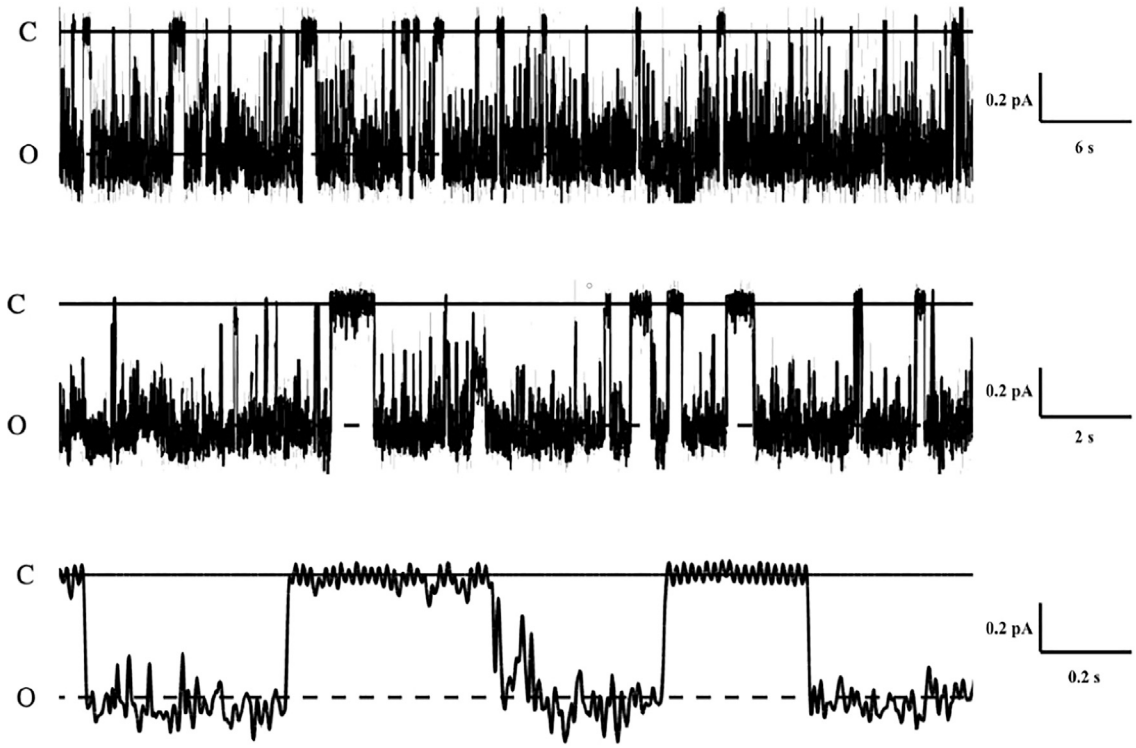

FIGURE 3 Representative WT-CFTR patch-clamp measurements on three different time scales.

sources associated with ATP_1 and ATP_2 are each labeled with $\frac{\Delta G_{LR}}{q}$. The energy associated with the binding of the ATP molecules is the Gibbs free energy associated with the ligand-receptor interaction between the particular ATP molecule and the portions of NBD_1 and NBD_2. Since volts equate to joules per coulomb, we can divide the Gibbs free energy by q, the charge on an electron, to obtain the voltage associated with this particular source in the circuit model. Ligand-receptor aspects of these sources are emphasized via the subscript LR for the sources in the circuit of Fig. 2. The resistors, R_1 and R_2 are a summing network for the input from ATP_1 and a noise source. The energy from ATP_2, through the resistor, R_3, is the other input to the AND gate, marked with an ampersand (&) in Fig. 2.

Much has been gleaned over the years in CFTR research from the membrane channel noise (55). The presence of a noise source in the model facilitates simulations of the CFTR channel response to the same. We have chosen to use BJTs, labeled Q in Fig. 2, for the active devices in the analog portion of the model. The output of the AND gate is then combined with another noise source through a summing network, comprising R_4 and R_5, before the input to the base of Q_1. Q_1 and Q_2 are in a configuration that is called a differential pair. This configuration only works in electronics if the transistors are perfectly matched, which is to say identical.

A multitude of aspects of CFTR can be incorporated into the digital portion of the model. In addition to the introduction of noise sources the internal design of the AND gate can be modified, for example by varying the thresholds at which the output of the AND gate goes low or high.

I_{CM} is the current which biases the differential pair into an active region of operation. In an actual analog circuit, this current would be generated by a current source and an associated current mirror. Q_3 is a split collector BJT and helps to ensure that under DC conditions, the collector currents being supplied to Q_1 and Q_2 are equal so that the differential pair is in perfect balance. Q_4 is a PNP BJT, which is biased with $\frac{1}{2}I_{CM}$ so that the collector voltages of Q_1 and Q_2 will be the same. In addition, the collector currents through Q_1 and Q_2 will be the collector current from half of the split collector and the base current from Q_3 and Q_4, respectively. It is imperative in analog integrated circuit design that components in associated circuits, such as differential pairs and current mirrors, be identical in their parameters and that they be biased with the same collector currents and collector voltages. As we will show, one of the ways one can think of this model is that in the WT CFTR the transistor components are matched and identical. In the various mutants they might not be identical components. It should be pointed out that for WT CFTR the structures of NBD_1 and NBD_2 are homologous, but not precisely identical. In contrast to the structure of the WT-CFTR channel, G551D-CFTR has a point mutation in the NBD_1 region, so for this variant it would be appropriate to map the NBD regions into a differential pair of Q_1 and Q_2, that are no longer perfectly matched.

One of the characteristics of a differential pair is that, in the normal region of operation, the inverting and non-inverting inputs are nominally at the same voltage. In our case this means that the voltage at the base of Q_1 is the same as the voltage at the base of Q_2. Because the base voltages are held at the same voltage, this can be used to refer to the input voltage at the base of Q_1 to the emitter of Q_5. The emitter current then drawn by Q_5 is given by

$$I_{e5} = \frac{\frac{\Delta G_{LR}}{q} - V_{cc}}{R_3}.$$

This current is then mirrored over to Q_7 from Q_6 and appears in Fig. 2 as I_{Cl^-}, the chloride current.

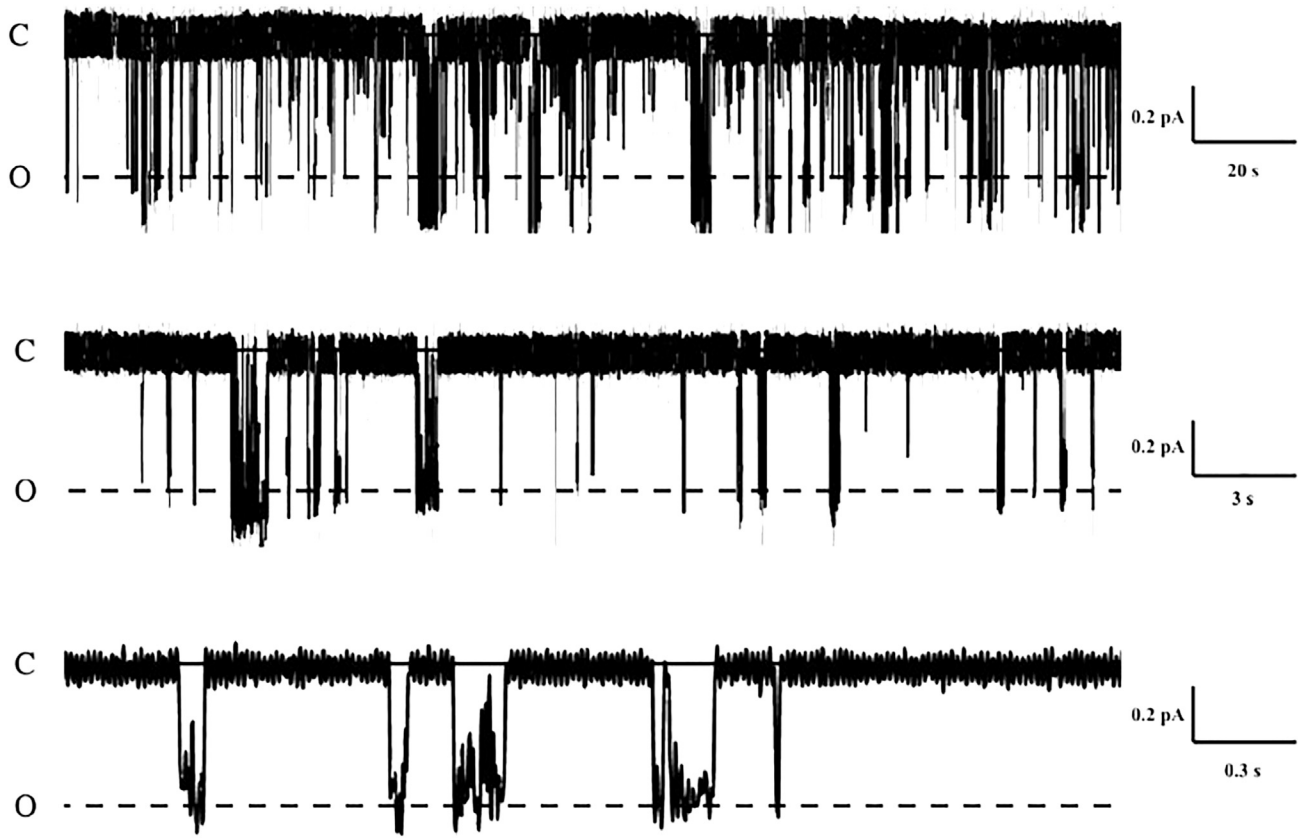

FIGURE 4 Representative G551D CFTR patch-clamp measurements on three different time scales.

Model for input source

When looking at the bibliography of ATP binding in CFTR (56–60), we see that the chemical kinetics of the two ATP molecules are very different. While one of the ATP molecules, ATP_1, has a very slow dissociation rate, remaining bound to CFTR for a long time, the other molecule, ATP_2, binds and dissociates from CFTR at a much faster rate—dissociating as ADP, if the ATP is hydrolyzed. Because of this difference in chemical kinetics, which ranges over several orders of magnitude (ATP_1 can stay bound for hundreds of seconds while ATP_2 stays on the order of milliseconds), we can disregard the effect of ATP_1 in our circuit model. We assume that it is always bound in our patch-clamp recordings, while the ATP_2 binds and unbinds relatively freely. With this assumption in hand, we can model the behavior of the binding of one ATP_2 to its binding site. The kinetic binding of an ATP to the NBD regions can hence be modeled as a Poisson process.

Initially, we theorized that there can be more than one state transition in this process—assuming a sum of exponentially distributed random variables. This yields an Erlang distribution with an unknown number of hidden states. However, after fitting the Erlang distribution to the open and closed times, we realized that the best fit was an Erlang distribution of order $n = 1$. This simplifies to an exponential distribution. Thus, we will use an exponentially distributed random variable to generate the open and closed times. The MATLAB code was used to generate a vector of 0s and 1s (closed or open states) with an average open time (τ_o) and closed time (τ_c) set to those metrics gleaned from the single-channel patch-clamp recordings. This output vector was then used as a model for the voltage sources $\frac{\Delta G_{LR}}{q}$ in Fig. 2. Also, the sampling frequency and the total duration time are variable in our code. The exponential distributions for the open and closed times are set to be independent of one another.

The noise in patch-clamp recordings is of great importance in understanding its nature. Although in some cases this noise is undesirable and reduces the accuracy of the measurements, in this case noise is an important component of the signal and should not be ignored. It is known that in CFTR noise there are components that are not from the measuring techniques but from the channels themselves, and these could give us some information about the protein structure, behavior, and mutations. To mimic in our model the noise observed in the patch-clamp measurements, we are utilizing two different noise sources with different components and objectives. First, we are including some Gaussian white noise after the AND gate (with R5 input resistance) that applies both to open and closed states. Moreover, it should be emphasized that the rate of ATP-NBD binding events is linearly dependent on the concentration of ATP, at least within the low-millimolar range, which is a key parameter of the model.

Noise

We used the white noise function from LTspice with amplitude of 1 V and set it in parallel to the output from the AND gate so that the voltage in the input node contains both the output signal from the AND gate and the noisy component from this noise source. This accounts for the uncertainty of the measurement as well as the small variations in the current through the CFTR with no distinction

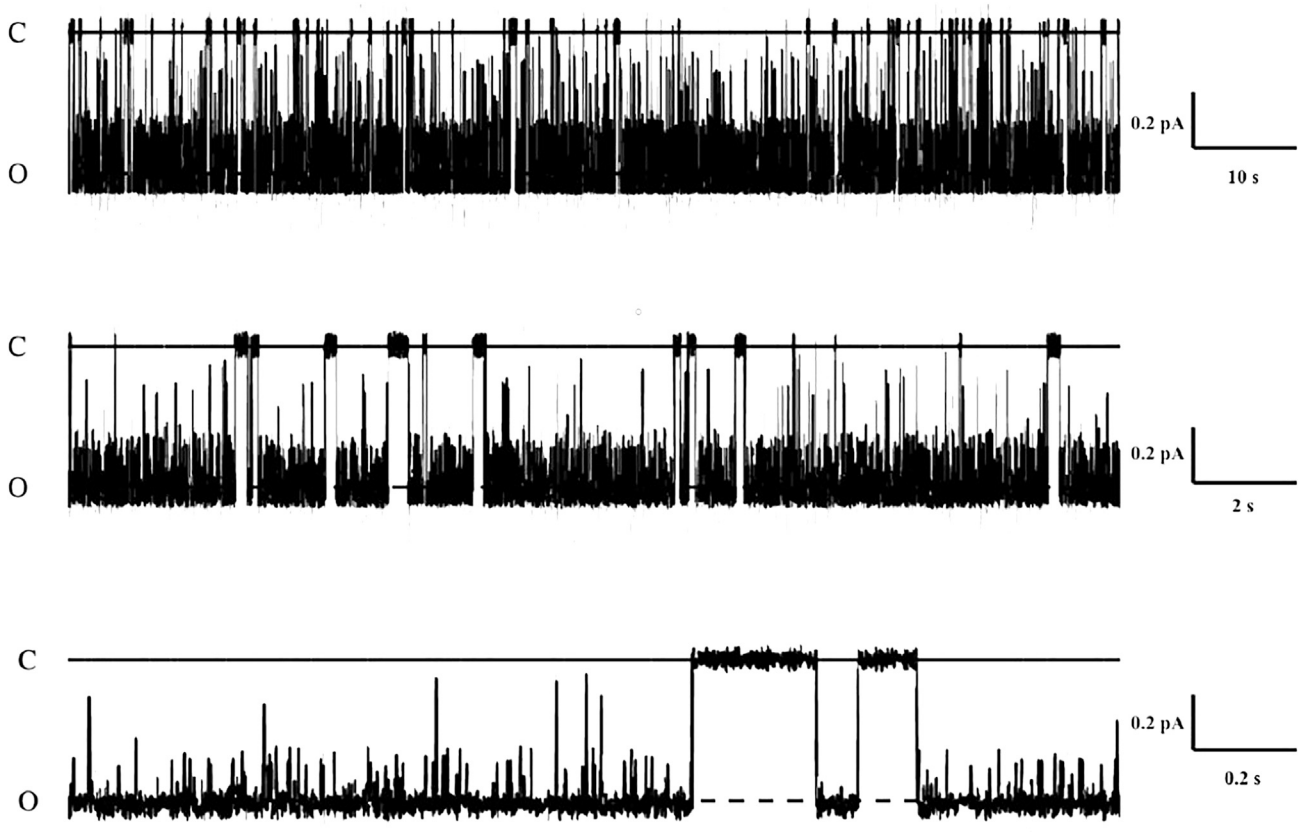

FIGURE 5 WT-CFTR model results at three time scales.

between the open and closed states. This helps make the signal more similar to the patch-clamp data.

As the ATP-NBD binding events depend on random interactions between ATP molecules in the environment and the NBD regions, the open durations of the circuit are random. Moreover, these interactions depend on whether the NBD is capable of receiving an ATP molecule and is already occupied by a previously bound ATP. Thus, the binding events have an inherently stochastic underpinning.

Between ATP-NBD events, CFTR proceeds through a sequence of transitions among hidden kinetic states before the NBD region is once again ready to accept ATP. The transitions may be modeled as a Poisson process. Thus, the total time taken for an opening or closing is the sum over the exponentially distributed random time between events. Assuming no recurrence (or rare recurrence) between states, and assuming the transitions between hidden states occur at roughly the same rates, the total time between ATP-NBD events takes on an Erlang distribution, with order equal to the number of state transitions in each opening and closing.

LTspice simulation and methodology

The circuit simulation tool we elected to use was LTspice. Our goal here is to map the protein structure of the CFTR membrane channel to the transistor circuit. The flexibility of this tool is important in being able modify some of the individual transistor parameters to more closely align with the biophysical consequences of CFTR mutations.

The default settings for the thresholds for the AND gate were used for virtually all of the modeled data in this paper. However, an additional attribute of LTspice is that the inner electronics of the AND gate can be modified readily to alter the thresholds at which the AND gate switches high and low. More is to be said about our use of this characteristic of the model and simulation tool in the flicker noise section of this paper.

The LTspice model is designed to predict the chloride channel current resulting from ATP binding so that we can obtain simulated patch-clamp data and be able to collect statistics associated with open and closing times and open probabilities.

An important attribute of this simulation tool, and many of the SPICE-based models, is that one can easily alter the characteristics of any transistor. Furthermore, programming languages internal to a circuit simulation tool, such as Verilog-A, can be used to incorporate both linear and nonlinear aspects of the transistor behavior. Given the complexity of the physics available within a transistor model, our approach should be seen as a technique complementary to molecular dynamics.

RESULTS

Measured patch-clamp data

Representative single-channel current traces of WT- and G551D-CFTR are shown in Figs. 3 and 4. We note that because the rate of G551D-CFTR activation is extremely low, we allowed G551D-CFTR to be activated by MgATP and PKA for only 10 min in order to

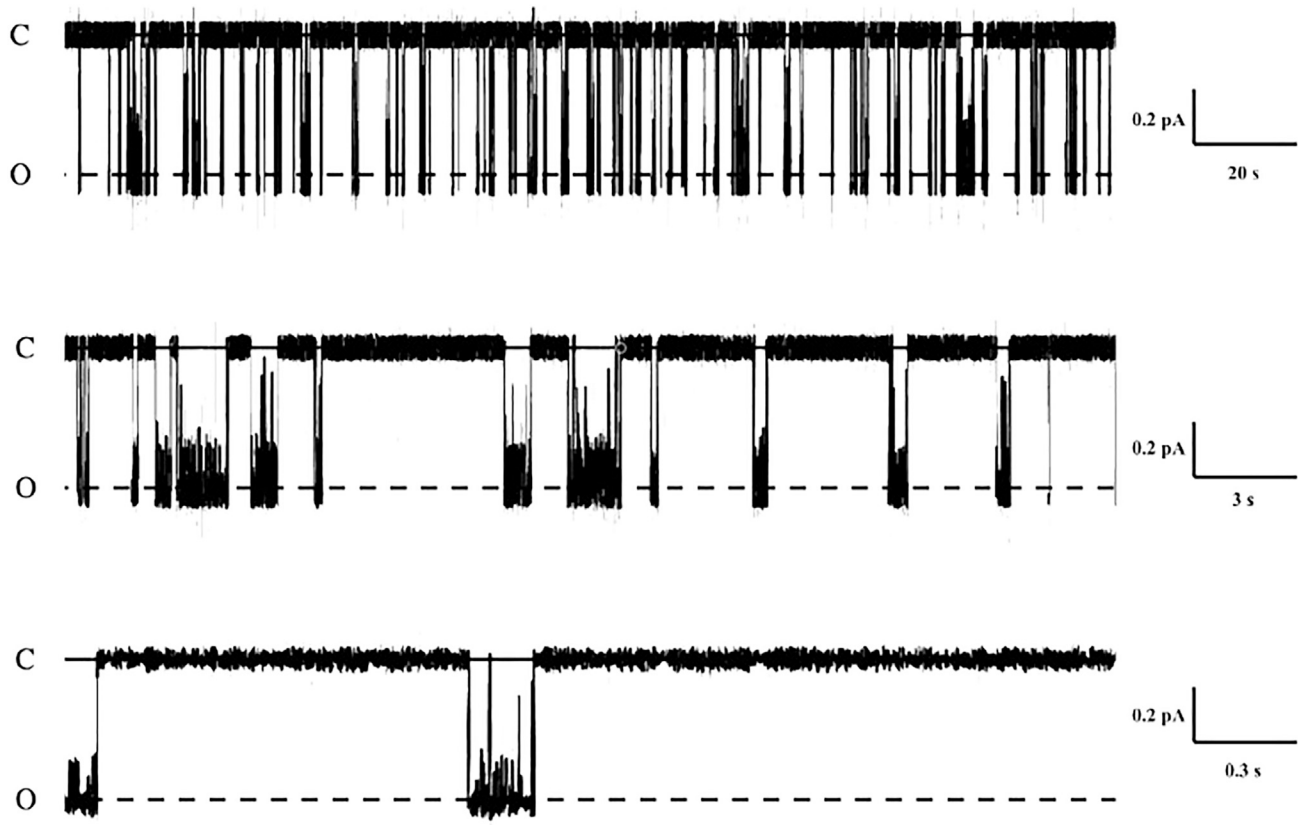

FIGURE 6 G551D-CFTR model results at three time scales.

maintain the high-quality seal resistance needed for these recordings. This is our standard protocol for single-channel patch-clamp recordings.

Model source characterization

One of the ATP molecules, ATP_1, is essentially always bound under physiological conditions, which is to say that this ATP-binding site #1 is always occupied by ATP at steady state. The interval between binding events at ATP-binding site #2 depends upon the ATP concentration in the solution. Assuming about 1 mM, which is close to the ATP concentration in normal cells at rest, the turnover rate for ATP is about 0.5 per second (9). We also know that WT CFTR has a typical open duration of 600 ms. If we assume that opening is very fast after binding of ATP and that closing is very fast after hydrolysis, which is not so well known, this is likely a good estimate of how long ATP is bound.

In the "model for input source" section, we noted that the times between ATP-NBD events could be modeled with an Erlang distribution. Moreover, since these events govern the opening of the channel, the time between events may be observed by measuring the time between channel openings. Given results such as those in Figs. 3 and 4, the mean of the Erlang distribution is chosen to match the average open and closed durations, as determined from the patch-clamp measurements.

Model results

We first seek a qualitative comparison of model data with the measured data to determine the efficacy of the model. In Fig. 5 we present the current output from the circuit model in LTspice for the WT-CFTR membrane channel showing open and closed states. The plotted current curves are not unlike the measured patch-clamp data that was shown in Fig. 3. In Fig. 5 we can see that the model can reproduce most of the characteristics of the measured signal, including the noise signal and the flickering in the open state. In Fig. 6 we present the model results for the G551D mutation and note that they are also similar to those obtained from patch-clamp measurements shown in Fig. 4. So in terms of the qualitative appearance, our model does a reasonable job of mimicking the patch-clamp behavior of the CFTR channel.

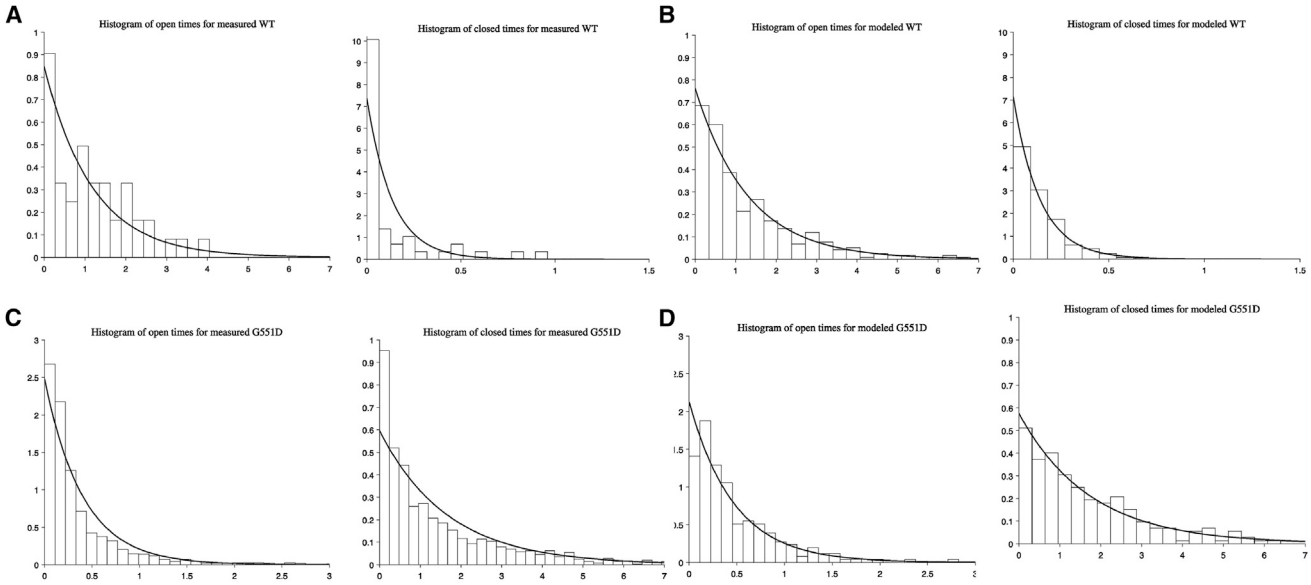

FIGURE 7 Histograms showing open and closing times: (*A*) WT measured, (*B*) WT modeled, (*C*) G551D measured, and (*D*) G551D modeled.

Statistical behavior of the model

Over the simulation of the WT-CFTR model for 100 s and for the measured patch-clamp data for the WT-CFTR membrane channels, we measured the open and closed durations using the standard methodology. The histograms for the open and closed times for the WT-CFTR measured data are shown in Fig. 7 *A*. The histograms for the open and closing times for the modeled WT CFTR are presented in Fig. 7 *B*. In Fig. 7 *C* we present the histograms for the patch-clamp measurements of the G551D mutant. Shown in Fig. 7 *D* are the open and closed time histograms for the modeled G551D mutation.

In Fig. 8 the histograms for the WT-CFTR channel, both the patch-clamp measurements and the model output, are presented. These histograms are used in standard practice to give us the opening and closing probabilities. In Fig. 9 we present the histograms for the G551D-CFTR mutation. Finally, we present the collected statistics for the patch-clamp measurements and the model results. Membrane channels are typically characterized by their open probability

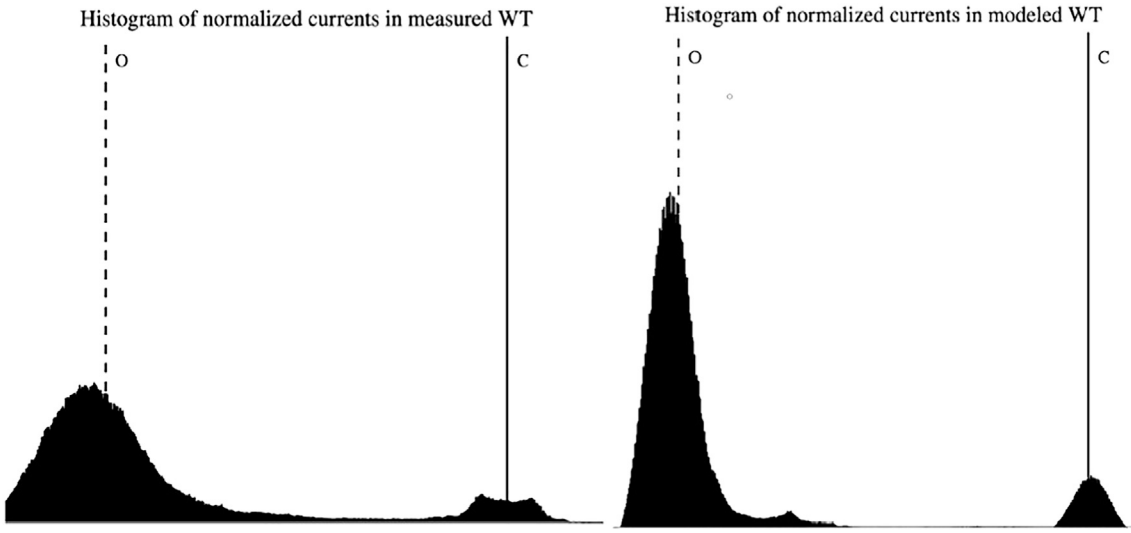

FIGURE 8 Histograms for WT measurement and model.

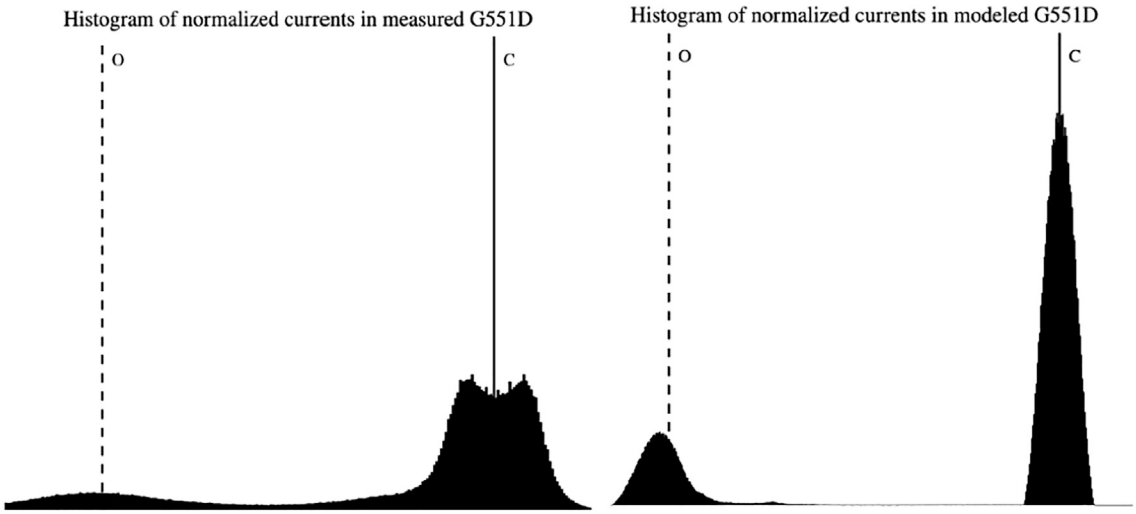

FIGURE 9 Histograms for G551D measurement and model.

P_o, open time (τ_o), and closed time (τ_c). These measurements are the usual statistical variables computed from patch-clamp measurements. The summary of all the statistical variables computed can be seen in Table 1, where they are shown for both the WT and the G551D-CFTR mutation.

Table 1 is key to understanding the success of our model. We can clearly see the similarity of all the statistical parameters in the measured data and the model, both in the WT and in the G551D mutant. This is the final quantitative demonstration that our model can reproduce the data and change depending on the parameters desired.

DISCUSSION

In this paper we have presented a mixed analog-digital circuit model for the CFTR membrane channel. In essence this circuit, presented in Fig. 2, is a voltage-to-current converter where in this case the driving voltage is the energy associated with ATP-binding events. The front end of the circuit is a logical AND gate which drives one transistor of a differential pair. This voltage is then referred over to the other transistor of the differential pair where that voltage sets up the current, which is then mirrored to the output as the chloride channel current. We used the model to simulate the chloride current in a WT-CFTR membrane channel and the G551D mutant of CFTR. One of the potential advantages of this model is that modification can be made in LTspice to the transistor parameters. There are roughly 2000 mutations of CFTR known, a good many of which are widely known with substantial single-channel patch-clamp measurements available. For example, there are mutations in the R domain which result in a lower number of phosphorylation sites and hence the supply voltage, $V_{R\ domain}$, which supplies a bias of sorts to the CFTR membrane channel, would be lowered.

TABLE 1 Mean values P_o, τ_o, and τ_c for WT and G551D measured and modeled

	Wild type		G551D	
	Measured	Modeled	Measured	Modeled
P_o	0.89	0.90	0.19	0.21
τ_o	1,170 ms	1,313 ms	403 ms	470 ms
τ_c	137 ms	140 ms	1,680 ms	1,735 ms

Flicker noise

The introduction of this noise source is one of the most novel aspects of this circuit model. This is done by adding a Gaussian white noise source in parallel with ATP_1, which creates some noise before the input to the AND gate. Then, and of critical importance, the thresholds of HIGH and LOW states in the AND gate model within LTspice were adjusted to be at a level inside the variance of the white noise. Without this noise source, the AND gate will always result in a HIGH output when ATP_1 is set to HIGH. However, in this case, when the ATP_1 is set to HIGH, the variability makes the output change between HIGH and LOW at very fast rates. The proportion of HIGH and LOW states depends on where this threshold is set. The resulting prediction of flicker noise is shown in Fig. 10 for three different thresholds for the AND gate. Flicker noise has for some time been observed in patch-clamp measurements of CFTR. Future efforts

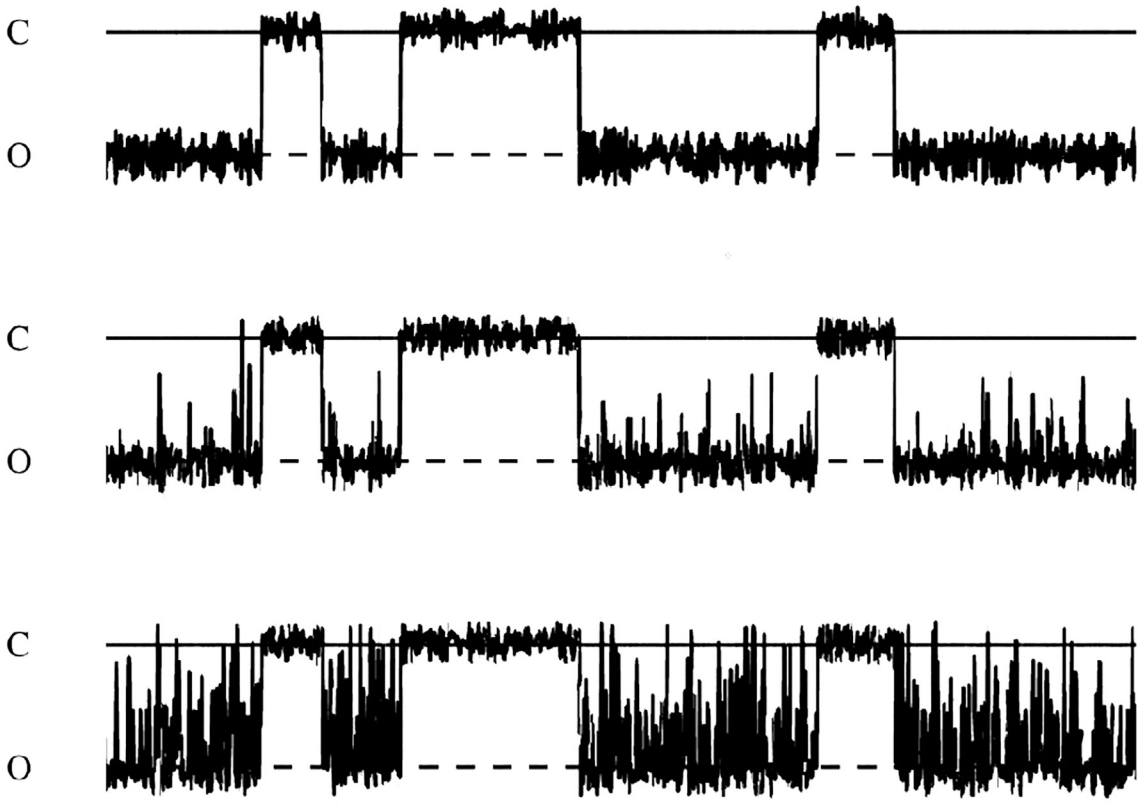

FIGURE 10 Flicker noise for three different thresholds for the AND gate.

will be directed at understanding this phenomenon better and what physiologically may be analogous to a modification of the AND gate threshold.

AUTHOR CONTRIBUTIONS

W.D.H. developed the circuit model and helped construct the Simulink (www.mathworks.com) model. N.A.M. provided the in-depth knowledge of CFTR which helped create and drive this work. E.M.M. developed the LTspice rendition of the circuit model and discovered the impact of modification of the AND gate threshold on flicker noise. R.S.W. provided high-level engineering understanding of the approach. P.R.Y. constructed an initial Simulink program version of the model. G.C. conducted the patch-clamp experiments. A.W.E. helped to create the source model and its stochastic nature, derived from experimental data. D.R.D. also provided high-level engineering understanding of the approach.

ACKNOWLEDGMENTS

This work has been supported under DARPA contract number HR001117C0124 as part of their RadioBio program. We wish to acknowledge the copy editing done on this article by David P. Thompson, a Ph.D. student in ECE at Georgia Tech.

DECLARATION OF INTERESTS

The authors declare no competing interests.

REFERENCES

1. Riordan, J. R., J. M. Rommens, …, J.-L. Chou. 1989. Identification of the cystic fibrosis gene: cloning and characterization of complementary DNA. *Science.* 245:1066–1073.
2. Rommens, J. M. 2011. Cystic Fibrosis Mutation Database. http://www.genet.sickkids.on.ca/app.
3. Sosnay, P. R., K. R. Siklosi, …, G. R. Cutting. 2013. Defining the disease liability of variants in the cystic fibrosis transmembrane conductance regulator gene. *Nat. Genet.* 45:1160–1167.
4. Kartner, N., J. W. Hanrahan, …, C. E. Bear. 1991. Expression of the cystic fibrosis gene in non-epithelial invertebrate cells produces a regulated anion conductance. *Cell.* 64:681–691.
5. Hyde, S. C., P. Emsley, …, C. F. Higgins. 1990. Structural model of ATP-binding proteing associated with cystic fibrosis, multidrug resistance and bacterial transport. *Nature.* 346:362–365.
6. Rees, D. C., E. Johnson, and O. Lewinson. 2009. ABC transporters: the power to change. *Nat. Rev. Mol. Cell Biol.* 10:218–227.
7. Infield, D. T., K. M. Strickland, …, N. A. McCarty. 2021. The molecular evolution of function in the CFTR chloride channel. *J. Gen. Physiol.* 153:e202012625.
8. Wang, W., and P. Linsdell. 2012. Alternating access to the transmembrane domain of the ATP-binding cassette protein cystic fibrosis transmembrane conductance regulator (ABCC7). *J. Biol. Chem.* 287:10156–10165.
9. Li, C., M. Ramjeesingh, W. Wang, …, C. E. Bear. 1996. ATPase activity of the cystic fibrosis transmembrane conductance regulator. *J. Biol. Chem.* 271:28463–28468.

10. Jardetzky, O. 1966. Simple allosteric model for membrane pumps. *Nature.* 211:969–970.
11. ter Beek, J., A. Guskov, and D. J. Slotboom. 2014. Structural diversity of ABC transporters. *J. Gen. Physiol.* 143:419–435.
12. Sebastian, A., L. Rishishwar, …, I. K. Jordan. 2013. Origin and evolution of the cystic fibrosis transmembrane regulator protein R domain. *Gene.* 523:137–146.
13. Baker, J. M. R., R. P. Hudson, …, J. D. Forman-Kay. 2007. CFTR regulatory region interacts with NBD1 predominantly via multiple transient helices. *Nat. Struct. Mol. Biol.* 14:738–745.
14. Hwang, T.-C., M. Horie, and D. C. Gadsby. 1993. Functionally distinct phospho-forms underlie incremental activation of protein kinase-regulated Cl-conductance in mammalian heart. *J. Gen. Physiol.* 101:629–650.
15. Dalemans, W., P. Barbry, …, M. Lazdunski. 1991. Altered chloride ion channel kinetics associated with the ΔF508 cystic fibrosis mutation. *Nature.* 354:526–528.
16. Denning, G. M., M. P. Anderson, …, M. J. Welsh. 1992. Processing of mutant cystic fibrosis transmembrane conductance regulator is temperature-sensitive. *Nature.* 358:761–764.
17. Drumm, M. L., D. J. Wilkinson, …, F. S. Collins. 1991. Chloride conductance expressed by delta F508 and other mutant CFTRs in Xenopus oocytes. *Science.* 254:1797–1799.
18. Sheppard, D. N., and M. J. Welsh. 1999. Structure and function of the CFTR chloride channel. *Physiol. Rev.* 79:S23–S45.
19. Hodgkin, A. L., and A. F. Huxley. 1952. A quantitative description of membrane current and its application to conduction and excitation in nerve. *J. Physiol.* 117:500–544. https://pubmed.ncbi.nlm.nih.gov/12991237.
20. Cronin, J., and J. C. Boutelle. 1987. Mathematical aspects of Hodgkin-Huxley neural theory. Cambridge University Press.
21. Brink, S., S. Nease, …, B. Degnan. 2013. A learning-enabled neuron array IC based upon transistor channel models of biological phenomena. *IEEE Trans. Biomed. Circuits Syst.* 7:71–81.
22. Mead, C. A., and M. A. Mahowald. 1988. A silicon model of early visual processing. *Neural Network.* 1:91–97.
23. Fitzhugh, R. 1960. Thresholds and plateaus in the Hodgkin-Huxley nerve equations. *J. Gen. Physiol.* 43:867–896.
24. Fox, R. F. 1997. Stochastic versions of the Hodgkin-Huxley equations. *Biophys. J.* 72:2068–2074.
25. Abbott, L., and T. B. Kepler. 1990. Model neurons: from hodgkin-huxley to hopfield. Springer, pp. 5–18.
26. Guckenheimer, J., and R. A. Oliva. 2002. Chaos in the Hodgkin–Huxley model. *SIAM J. Appl. Dyn. Syst.* 1:105–114.
27. Kistler, W. M., W. Gerstner, and J. L. v. Hemmen. 1997. Reduction of the Hodgkin-Huxley equations to a single-variable threshold model. *Neural Comput.* 9:1015–1045.
28. Goldwyn, J. H., and E. Shea-Brown. 2011. The what and where of adding channel noise to the Hodgkin-Huxley equations. *PLoS Comput. Biol.* 7:e1002247.
29. Catterall, W. A., I. M. Raman, …, O. Paulsen. 2012. The Hodgkin-Huxley heritage: from channels to circuits. *J. Neurosci.* 32:14064–14073.
30. Ullah, G., and S. J. Schiff. 2009. Tracking and control of neuronal Hodgkin-Huxley dynamics. *Phys. Rev.* 79:040901.
31. Moujahid, A., A. d'Anjou, …, F. Torrealdea. 2011. Energy and information in Hodgkin-Huxley neurons. *Phys. Rev.* 83:031912.
32. Häusser, M. 2000. The Hodgkin-Huxley theory of the action potential. *Nat. Neurosci.* 3:1165.
33. Meunier, C., and I. Segev. 2002. Playing the Devil's advocate: is the Hodgkin–Huxley model useful? *Trends Neurosci.* 25:558–563.
34. Cole, K. S., and H. J. Curtis. 1939. Electric impedance of the squid giant axon during activity. *J. Gen. Physiol.* 22:649–670.
35. Hodgkin, A. L., and A. F. Huxley. 1952. Currents carried by sodium and potassium ions through the membrane of the giant axon of Loligo. *J. Physiol.* 116:449–472.
36. Hodgkin, A. L., and A. F. Huxley. 1952. The components of membrane conductance in the giant axon of Loligo. *J. Physiol.* 116:473–496.
37. Hodgkin, A. L., and A. F. Huxley. 1952. The dual effect of membrane potential on sodium conductance in the giant axon of Loligo. *J. Physiol.* 116:497–506.
38. Hodgkin, A. L., A. F. Huxley, and B. Katz. 1952. Measurement of current-voltage relations in the membrane of the giant axon of Loligo. *J. Physiol.* 116:424–448.
39. Hamill, O. P., A. Marty, …, F. J. Sigworth. 1981. Improved patch-clamp techniques for high-resolution current recording from cells and cell-free membrane patches. *Pflugers Arch.* 391:85–100.
40. Bardeen, J., and W. H. Brattain. 1948. The transistor, a semiconductor triode. *Phys. Rev.* 74:230–231.
41. Ayaz, M., and S. B. Yanardag. 2017. Potassium Channels: A Transistor Model. *J. Adv. Neurosci. Res.* 4:14–18.
42. Eisenberg, B. 1994. Biological signals that need detection: Currents through single membrane channels. *In* Proceedings of 16th Annual International Conference of the IEEE Engineering in Medicine and Biology Society IEEE, pp. 724–725.
43. Eisenberg, B. 1998. Ionic channels in biological membranes: natural nanotubes. *Acc. Chem. Res.* 31:117–123.
44. Eisenberg, B. 1998. Ionic channels in biological membranes-electrostatic analysis of a natural nanotube. *Contemp. Phys.* 39:447–466.
45. Eisenberg, B. 2005. Living transistors: a physicist's view of ion channels. Preprint at arXiv. http://arxiv.org/abs/q-bio/0506016v2.
46. Horng, T.-L., T.-C. Lin, …, B. Eisenberg. 2012. PNP equations with steric effects: a model of ion flow through channels. *J. Phys. Chem. B.* 116:11422–11441.
47. Hynna, K. M., and K. Boahen. 2007. Thermodynamically equivalent silicon models of voltage-dependent ion channels. *Neural Comput.* 19:327–350.
48. Lemeshko, V. V., and S. V. Lemeshko. 2004. The voltage-dependent anion channel as a biological transistor: theoretical considerations. *Eur. Biophys. J.* 33:352–359.
49. Cui, G., C. S. Freeman, …, N. A. McCarty. 2013. Two salt bridges differentially contribute to the maintenance of cystic fibrosis transmembrane conductance regulator (CFTR) channel function. *J. Biol. Chem.* 288:20758–20767.
50. Cui, G., and N. A. McCarty. 2015. Murine and human CFTR exhibit different sensitivities to CFTR potentiators. *Am. J. Physiol. Lung Cell Mol. Physiol.* 309:L687–L699.
51. Cui, G., N. Khazanov, …, N. A. McCarty. 2016. Potentiators exert distinct effects on human, murine, and Xenopus CFTR. *Am. J. Physiol. Lung Cell Mol. Physiol.* 311:L192–L207.
52. Cui, G., K. A. Cottrill, and N. A. McCarty. 2021. Electrophysiological Approaches for the Study of Ion Channel Function. *Methods Mol. Biol.* 2302:49–67.
53. Rahman, K. S., G. Cui, …, N. A. McCarty. 2013. Modeling the conformational changes underlying channel opening in CFTR. *PLoS One.* 8:e74574.
54. Strickland, K. M., G. Stock, …, J. C. Gumbart. 2019. ATP-dependent signaling in simulations of a revised model of cystic fibrosis transmembrane conductance regulator (CFTR). *J. Phys. Chem. B.* 123:3177–3188.
55. DeFelice, L. J. 1981. Introduction to Membrane Noise. Springer.
56. Yeh, H.-I., Y.-C. Yu, …, T.-C. Hwang. 2021. Functional stability of CFTR depends on tight binding of ATP at its degenerate ATP-binding site. *J. Physiol.* 599:4625–4642.

57. Lin, W.-Y., K.-Y. Jih, and T.-C. Hwang. 2014. A single amino acid substitution in CFTR converts ATP to an inhibitory ligand. *J. Gen. Physiol.* 144:311–320.

58. Shimizu, H., Y.-C. Yu, …, Y. Sohma. 2010. A stable ATP binding to the nucleotide binding domain is important for reliable gating cycle in an ABC transporter CFTR. *J. Physiol. Sci.* 60:353–362.

59. Stratford, F. L. L., M. Ramjeesingh, …, C. E. Bear. 2007. The Walker B motif of the second nucleotide-binding domain (NBD2) of CFTR plays a key role in ATPase activity by the NBD1–NBD2 heterodimer. *Biochem. J.* 401:581–586.

60. Zhou, Z., X. Wang, …, T.-C. Hwang. 2006. The two ATP binding sites of cystic fibrosis transmembrane conductance regulator (CFTR) play distinct roles in gating kinetics and energetics. *J. Gen. Physiol.* 128:413–422.